ETH
Eidgenössische Technische Hochschule Zürich
Swiss Federal Institute of Technology Zurich

Seminar for Applied Mathematics SAM

A Second-Kind Galerkin Boundary Element Method for Scattering at Composite Objects

X. Claeys and R. Hiptmair and E. Spindler

Research Report No. 2013-13
April 2013

Seminar für Angewandte Mathematik
Eidgenössische Technische Hochschule
CH-8092 Zürich
Switzerland

- Funding SNF: 20021_137873/1

BIT manuscript No.
(will be inserted by the editor)

A Second-Kind Galerkin Boundary Element Method for Scattering at Composite Objects

Xavier Claeys*, Ralf Hiptmair†, and Elke Spindler†

May 12, 2013

Abstract We consider the scattering of time-harmonic acoustic waves at objects composed of several homogeneous parts with different material properties. In [X. Claeys, *A single trace integral formulation of the second kind for acoustic scattering*, Report 2011-14, SAM, ETH Zürich] a novel second-kind boundary integral formulation for this scattering problem was proposed. We recast it into a variational problem set in L^2 and investigate its Galerkin boundary element discretization from a theoretical and algorithmic point of view. Empiric studies demonstrate the competitive accuracy and superior conditioning of the new approach compared to a widely used Galerkin boundary element approach based on a first-kind boundary integral formulation.

Keywords Acoustic scattering, second-kind boundary integral equations, Galerkin boundary element methods

Mathematics Subject Classification (2000) 65N12, 65N38, 65R20

1 Acoustic scattering at Composite Obstacles

We consider the scattering of an incident acoustic wave at a bounded penetrable obstacle composed of several homogeneous parts. To give a precise description, we write $\Omega_* \subset \mathbb{R}^d$, $d = 2, 3$, for the domain occupied by the obstacle, and introduce its parts as open sub-domains $\Omega_i \subset \mathbb{R}^d$, $i = 1, \ldots, N$, that form a partition of Ω_* in the sense that $\Omega_i \cap \Omega_j = \emptyset$ for $j \neq i$ and $\overline{\Omega}_* = \bigcup_{i=1}^N \overline{\Omega}_i$. Both Ω_* and all Ω_i are supposed to be connected Lipschitz domains [10], which also applies to the unbounded complement $\Omega_0 := \mathbb{R}^d \setminus \overline{\Omega}_*$.

The generic situation that we have in mind (for $d = 2$) is sketched in Figure 1.1. We call points where three or more sub-domains abut "material

* Laboratoire Jacques-Louis Lions, Paris IV, France, email: xavier.claeys@upmc.fr
† Seminar for Applied Mathematics, Swiss Federal Institute of Technology, Zurich, Switzerland, emails: {hiptmair,elke.spindler}@sam.math.ethz.ch. The work of E. Spindler was partially supported by SNF under grant 20021_137873/1.

junction points" (marked as ● in Figure 1.1). In those regions some sub-domains Ω_i will inevitably have non-smooth boundaries. For each $i = 1, \dots, N$, the boundary $\partial\Omega_i$ can be endowed with a unit normal vector field $\mathbf{n}_i$ pointing into the exterior of Ω_i. We write Γ_{ij} for the common interface of Ω_i and Ω_j, $\Gamma_{ij} := \partial\Omega_i \cap \partial\Omega_j$, $i \neq j$. The union of all the interfaces Γ_{ij} forms the so-called *skeleton* $\Sigma := \bigcup_{j<i} \Gamma_{ij} = \bigcup_{i=0}^{N} \partial\Omega_i$.

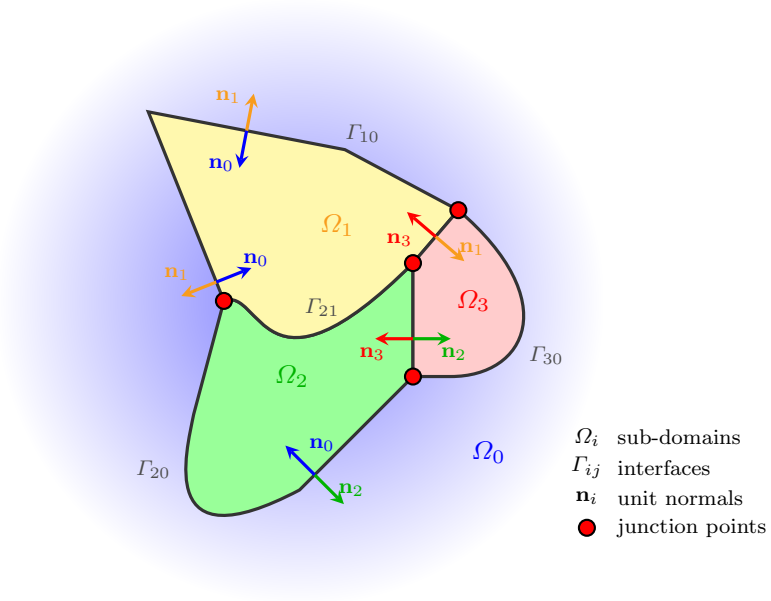

Fig. 1.1: Typical geometry of a composite scatterer for $N = 3$.

In the context of acoustic scattering, each sub-domain is filled with a medium characterized by a local wave number $\kappa_i \in \mathbb{R}_+$, $i = 0, \dots, N$. These are lumped together into the piecewise constant coefficient function $\kappa \in L^\infty(\mathbb{R}^d)$, $\kappa_{|\Omega_i} \equiv \kappa_i$. Sources will be introduced into our scattering model through a given *incident wave* $U_{\mathrm{inc}} \in C^\infty(\mathbb{R}^d)$ that satisfies[1]

$$-\Delta U_{\mathrm{inc}} - \kappa_0^2 U_{\mathrm{inc}} = 0 \quad \text{everywhere in } \mathbb{R}^d\,. \tag{1.1}$$

In many applications U_{inc} will be a plane wave. Then, the acoustic scattering problem consists in looking for a $U \in H^1_{\mathrm{loc}}(\mathbb{R}^d)$ such that[2]

$$\int_{\mathbb{R}^d} \mathbf{grad}\, U(\boldsymbol{x}) \cdot \mathbf{grad}\, V(\boldsymbol{x}) - \kappa^2(\boldsymbol{x}) U(\boldsymbol{x}) V(\boldsymbol{x})\, \mathrm{d}\boldsymbol{x} = 0 \quad \forall V \in H^1_{\mathrm{comp}}(\mathbb{R}^d)\,, \tag{1.2a}$$

[1] Capital letters are used to refer to functions defined over a volume domain.

[2] Notations for function spaces follow the usual conventions, see [7, 16]

$$\lim_{r\to\infty} \int\limits_{|\boldsymbol{x}|=r} \left| \mathbf{grad}(U - U_{\mathrm{inc}}) \cdot \frac{\boldsymbol{x}}{|\boldsymbol{x}|} - \mathrm{i}\kappa_0 (U - U_{\mathrm{inc}})(\boldsymbol{x}) \right|^2 \mathrm{d}S(\boldsymbol{x}) = 0 \,. \tag{1.2b}$$

Existence and uniqueness of solutions of (1.2) is well established [4, 13]. We also point out that (1.2) is equivalent to a transmission problem for the homogeneous Helmholtz equations $-\Delta U - \kappa_i^2 U = 0$, see [7, Sect. 1.2], and that (1.2b) expresses the so-called Sommerfeld radiation conditions [8, Sect. 2.2].

Remark 1.1 (Discontinuous "diffusion coefficient") *What about admitting a piecewise constant coefficient also in the second-order part of the bilinear form in* (1.2a)*? Alas, this will lead to transmission problems that are* outside the scope of the method *discussed in this article, because serendipitous cancellations of singularities of the integral kernel will no longer occur, see Section 4.3.* △

2 Introduction

In the case of acoustic scattering with piecewise homogeneous material described above low-order Galerkin boundary element methods (BEM) are a very attractive option for the approximate numerical solution of (1.2). They can easily cope with unbounded domains and, in contrast to finite element methods, can dispense with volume meshes.

Galerkin BEM rely on boundary integral equations (BIE) in variational form. The classical approach to obtain those for (1.2) is the so-called first-kind single trace trace formulation (STF), introduced in [23]. In computational electromagnetics the STF is known as PMCHWT [12,18], see also [7, Sect. 3]. Unfortunately, its Galerkin discretization by means of low order boundary elements leads to ill-conditioned linear systems on fine meshes, and the popular operator preconditioning strategy ("Calderón preconditioning") does not seem to be available [7, Sect. 4]. On the other hand, effective preconditioning becomes mandatory, when the sheer problem size demands matrix compression, and, as a consequence, the use of iterative solvers.

In contrast to first-kind BIE, the so-called second-kind boundary integral equations readily yield well-conditioned linear systems. For $N = 1$, that is, the case of two materials separated by a closed interface, such formulations for (1.2) are well-known, see [5,15,17,19]. Yet, for a long time it remained obscure how to extend them to situations with junction points. Only recently, in [6] and the parallel work [11], a breakthrough was achieved by considering *total potentials*, see Section 3.3 below.

In this article we follow the approach of [6] and extend it to obtain a second-kind variational BIE set in $L^2(\Sigma)$, see Section 3.4. We carefully examine the arising non-standard boundary integral operators both in terms of structural properties and numerical treatment, see Section 4. Numerical tests in two dimensions, reported in Section 5, bolster the conjectured unconditional stability of the new formulation and confirm the predicted asymptotic

algebraic rates of convergence. They also demonstrate that the new method matches the accuracy obtained with STF-based BEM. We point out that our approach has little in common with [11], where a Nystrom discretization was pursued.

3 Second-Kind Boundary Integral Formulation

3.1 Traces and Potentials

Fixing the sub-domain Ω_i, we recall the Dirichlet trace $\gamma_D^i : H^1_{\mathrm{loc}}(\Omega_i) \to H^{\frac{1}{2}}(\partial\Omega_i)$, extending the pointwise restriction of smooth functions to $\partial\Omega_i$, and the Neumann trace (co-normal trace), $\gamma_N^i : H^1_{\mathrm{loc}}(\Delta, \overline{\Omega_i}) \to H^{-\frac{1}{2}}(\partial\Omega_i)$, $\gamma_N^i := \mathbf{n}_i \cdot \begin{pmatrix}\gamma_D^i \\ \gamma_D^i\end{pmatrix} \circ \mathbf{grad}$, *cf.*, e.g., [20, Theorems 2.6.9, 2.8.3 & Lemma 2.8.4]. The associated trace spaces, henceforth called "Dirichlet trace space" and "Neumann trace space", can be merged into the Cauchy trace space

$$\mathcal{H}(\partial\Omega_i) := H^{\frac{1}{2}}(\partial\Omega_i) \times H^{-\frac{1}{2}}(\partial\Omega_i)\,, \tag{3.1}$$

which is *self-dual* with respect to the pairing [3]

$$\langle\!\langle \mathfrak{u}, \mathfrak{v} \rangle\!\rangle_{\mathcal{H}(\partial\Omega_i)} := \langle u, \varphi\rangle_{\partial\Omega_i} + \langle v, \nu\rangle_{\partial\Omega_i}\,,\ \mathfrak{u} := \begin{pmatrix} u \\ \nu \end{pmatrix},\ \mathfrak{v} := \begin{pmatrix} v \\ \varphi \end{pmatrix} \in \mathcal{H}(\partial\Omega_i)\,, \tag{3.2}$$

with $\langle\cdot,\cdot\rangle_{\Omega_i}$ denoting (extensions of) the L^2-duality pairing on $\partial\Omega_i$. A related compact notation is the Cauchy trace operator

$$\gamma^i : H^1_{\mathrm{loc}}(\Delta, \Omega_i) \to \mathcal{H}(\partial\Omega_i)\,, \quad \gamma^i U := \begin{pmatrix} \gamma_D^i U \\ \gamma_N^i U \end{pmatrix}. \tag{3.3}$$

Potential representations of solutions of (1.2) are the first step towards boundary integral equations. The following result can be found in [20, Sect. 3.11] and [16, Ch. 6]:

Theorem 3.1 (Single domain representation formula) *There are continuous operators, depending on the constant $\kappa > 0$, the*

$$\begin{aligned} &\textit{single layer potential} && \mathbb{S}_i[\kappa] : H^{-\frac{1}{2}}(\partial\Omega_i) \to H^1_{\mathrm{loc}}(\Delta, \mathbb{R}^d \setminus \partial\Omega_i)\,, \\ &\textit{double layer potential} && \mathbb{D}_i[\kappa] : H^{\frac{1}{2}}(\partial\Omega_i) \to H^1_{\mathrm{loc}}(\Delta, \mathbb{R}^d \setminus \partial\Omega_i)\,, \end{aligned}$$

such that

(i) $\mathbb{S}_i[\kappa](\varphi)$ and $\mathbb{D}_i[\kappa](u)$ satisfy $-\Delta \cdot -\kappa^2 \cdot = 0$ in $\Omega_i \cup \mathbb{R}^2 \setminus \overline{\Omega_i}$ and the Sommerfeld radiation conditions (1.2b) for any $\varphi \in H^{-\frac{1}{2}}(\partial\Omega_i)$, $u \in H^{\frac{1}{2}}(\partial\Omega_i)$.

[3] Fraktur font is used to designate functions in the Cauchy trace space, whereas Roman typeface is reserved for Dirichlet traces, and Greek symbols for Neumann traces.

(ii) Every solution $U \in H^1_{\mathrm{loc}}(\Omega_i)$ *of* $\left(-\Delta - \kappa^2\right) U = 0$ *that satisfies the Sommerfeld radiation conditions if* $i = 0$ *fulfills*

$$\mathbb{G}_i[\kappa](\gamma^i U) = \begin{cases} U & \text{on } \Omega_i \,, \\ 0 & \text{on } \mathbb{R}^d \backslash \overline{\Omega_i} \,, \end{cases} \tag{3.4}$$

with the local total potentials *defined by*

$$\mathbb{G}_i[\kappa](\mathfrak{u}) := -\mathbb{D}_i[\kappa](u) + \mathbb{S}_i[\kappa](\varphi) \,, \quad \mathfrak{u} := \begin{pmatrix} u \\ \varphi \end{pmatrix} \in \mathcal{H}(\partial\Omega_i) \,.$$

For functions φ and u on $\partial\Omega_i$ the potentials possess the integral representations

$$\begin{aligned} \mathbb{S}_i[\kappa](\varphi)(\boldsymbol{x}) &= \int_{\partial\Omega_i} \Phi_\kappa(\boldsymbol{x} - \boldsymbol{y})\, \varphi(\boldsymbol{y})\, \mathrm{d}S(\boldsymbol{y}) \,, \\ \mathbb{D}_i[\kappa](u)(\boldsymbol{x}) &= \int_{\partial\Omega_i} \mathbf{grad}_{\boldsymbol{y}}\, \Phi_\kappa(\boldsymbol{x} - \boldsymbol{y}) \cdot \boldsymbol{n}_i(\boldsymbol{y})\, u(\boldsymbol{y})\, \mathrm{d}S(\boldsymbol{y}) \,, \end{aligned} \tag{3.5}$$

for $\boldsymbol{x} \notin \partial\Omega_i$, with the fundamental solutions

$$\Phi_\kappa(\boldsymbol{z}) = \begin{cases} \frac{\mathrm{i}}{4} H_0^{(1)}(\kappa\,|\boldsymbol{z}|), & d = 2 \\ \frac{1}{4\pi|\boldsymbol{z}|} \exp(\mathrm{i}\kappa\,|\boldsymbol{z}|), & d = 3 \end{cases} , \quad \kappa \in \mathbb{R}_+ \,, \tag{3.6}$$

where $H_0^{(1)}$ is the Hankel function of the first kind and $|\cdot|$ represents the Euclidean norm.

Notations. For simplicity we neglect the argument $[\kappa]$ in $\mathbb{S}_i[\kappa]$, $\mathbb{D}_i[\kappa]$, and $\mathbb{G}_i[\kappa]$ and write $\mathbb{S}_i$, $\mathbb{D}_i$, $\mathbb{G}_i$, respectively, in the cases where κ in the formulas (3.5) coincides with the local wave number κ_i of Ω_i.

3.2 Skeleton trace spaces

Definition 3.1 (Multi-trace space) The skeleton *multi-trace space* is defined as the product of local Cauchy trace spaces

$$\boldsymbol{\mathcal{MT}}(\Sigma) := \bigtimes_{i=0}^{N} \mathcal{H}(\partial\Omega_i) \,. \tag{3.7}$$

It owes its name to the fact that on each interface Γ_{ij} a function $\mathfrak{u} \in \boldsymbol{\mathcal{MT}}(\Sigma)$ comprises two pairs of Dirichlet and Neumann data, one contributed by the sub-domain on either side. Based on Cauchy traces (3.3) we define the skeleton multi-trace operator γ^Σ, which maps $H^1_{\mathrm{loc}}(\Delta, \mathbb{R}^d)$ into the multi-trace space:

$$\gamma^\Sigma : \; H^1_{\mathrm{loc}}(\Delta, \mathbb{R}^d) \to \boldsymbol{\mathcal{MT}}(\Sigma) \,, \; U \mapsto \gamma^\Sigma U \quad := (\gamma^0 U, \gamma^1 U, ..., \gamma^N U) \,. \tag{3.8}$$

Self-duality of $\boldsymbol{\mathcal{MT}}(\Sigma)$ is induced by the following L^2-type bi-linear pairing (3.2); for $\mathfrak{u} = (\mathfrak{u}_0, ..., \mathfrak{u}_N)$, $\mathfrak{v} = (\mathfrak{v}_0, ..., \mathfrak{v}_N) \in \boldsymbol{\mathcal{MT}}(\Sigma)$ we define

$$\langle\!\langle \mathfrak{u}, \mathfrak{v} \rangle\!\rangle := \sum_{i=0}^{N} \langle\!\langle \mathfrak{u}_i, \mathfrak{v}_i \rangle\!\rangle_{\mathcal{H}(\partial\Omega_i)} \,. \tag{3.9}$$

For sufficiently smooth functions we can rewrite (3.9) using the fact that each interface is visited twice when summing integrals over all sub-domain boundaries:

$$\langle\!\langle \mathfrak{u}, \mathfrak{v} \rangle\!\rangle = \sum_{j<i} \int_{\Gamma_{ij}} u_i \overline{\psi_i} + \nu_i \overline{v_i} + u_j \overline{\psi_j} + \nu_j \overline{v_j} \, \mathrm{d}S \,, \tag{3.10}$$

where $\mathfrak{u}_i = (u_i, \nu_i)$, $\mathfrak{v}_i = (v_i, \psi_i)$.

Next, we introduce the important subspace of unique traces in $\boldsymbol{\mathcal{MT}}(\Sigma)$:

Definition 3.2 (Single-trace space)

$$\boldsymbol{\mathcal{ST}}(\Sigma) := \Big\{ (u_0, \nu_0, \dots, u_N, \nu_N) \in \boldsymbol{\mathcal{MT}}(\Sigma) : \\ \exists U \in H^1(\mathbb{R}^d),\ u_i = \gamma_D^i U,\ \exists \boldsymbol{\phi} \in \boldsymbol{H}(\mathrm{div}, \mathbb{R}^d),\ \nu_i = \boldsymbol{n}_i \cdot \boldsymbol{\phi} \Big\} \,.$$

In words, functions in $\boldsymbol{\mathcal{ST}}(\Sigma)$ are skeleton traces of functions defined everywhere on $\mathbb{R}^d$. The *transmission conditions* inherent in the variational formulation (1.2a) imply for the solution U of (1.2):

$$U \text{ solves (1.2a)} \quad \Rightarrow \quad \gamma^\Sigma U \in \boldsymbol{\mathcal{ST}}(\Sigma) \,. \tag{3.11}$$

Another fundamental result is the following "polar set" characterization of $\boldsymbol{\mathcal{ST}}(\Sigma)$ as a subspace of $\boldsymbol{\mathcal{MT}}(\Sigma)$, see [6, Prop. 2.1] and [7, Thm. 3.1],

$$\boldsymbol{\mathcal{ST}}(\Sigma) = \{ \mathfrak{u} \in \boldsymbol{\mathcal{MT}}(\Sigma) :\ \langle\!\langle \mathfrak{u}, \mathfrak{v} \rangle\!\rangle = 0,\ \forall \mathfrak{v} \in \boldsymbol{\mathcal{ST}}(\Sigma) \} \,. \tag{3.12}$$

3.3 Multi-potentials

Definition 3.3 (multi-potential) The *multi-potential* is defined as the sum over all total local potentials $\mathbb{G}_i[\kappa_i]$ defined in Theorem 3.1, $i = 0, ..., N$:

$$\mathbb{M}_\Sigma : \boldsymbol{\mathcal{MT}}(\Sigma) \to H^1_{\mathrm{loc}}(\Delta, \mathbb{R}^d \setminus \Sigma), \quad \mathbb{M}_\Sigma(\mathfrak{u}) := \sum_{i=0}^{N} \mathbb{G}_i[\kappa_i](\mathfrak{u}_i) \,. \tag{3.13}$$

An immediate consequence of equation (3.4) is

Corollary 3.1 (Global Representation Formula) *Let U solve the transmission problem (1.2), then*

$$U - \chi_{\Omega_0} U_{\mathrm{inc}} = \mathbb{M}_\Sigma(\gamma^\Sigma U - (\gamma^0 U_{\mathrm{inc}}, 0, \dots, 0)) \,, \tag{3.14}$$

where γ^Σ is the multi-trace defined in (3.8) and χ_{Ω_0} is the characteristic function of Ω_0.

We define the boundary integral operator $\mathbf{M}_\Sigma$ by taking the skeleton trace of (3.13):

Definition 3.4 (Multi Boundary Integral Operator)

$$\mathsf{M}_\Sigma := \gamma^\Sigma \mathbb{M}_\Sigma : \quad \boldsymbol{\mathcal{MT}}(\Sigma) \quad \to \quad \boldsymbol{\mathcal{MT}}(\Sigma)\,. \tag{3.15}$$

Notations. If $\mathbb{M}_\Sigma$ or M_Σ are supplied with an argument $[\kappa]$, all wave numbers κ_i in (3.13) are supposed to agree with κ in $\mathbb{M}_\Sigma[\kappa]$ and $\mathsf{M}_\Sigma[\kappa]$, respectively.

Next, we derive boundary integral equations from (3.14). We apply the skeleton trace to it and test the resulting equation with $\mathfrak{v} \in \boldsymbol{\mathcal{MT}}(\Sigma)$, which gives us a boundary integral equation in variational form:

Formulation 3.1 *Search* $\mathfrak{u} \in \boldsymbol{\mathcal{ST}}(\Sigma)$:

$$\langle\!\langle (\mathsf{Id} - \mathsf{M}_\Sigma)\mathfrak{u}, \mathfrak{v}\rangle\!\rangle = \langle\!\langle \mathfrak{u}_{\rm inc}, \mathfrak{v}\rangle\!\rangle\ , \quad \forall \mathfrak{v} \in \boldsymbol{\mathcal{MT}}(\Sigma), \tag{3.16}$$

where $\mathfrak{u}_{\rm inc} := \gamma_\Sigma U_{\rm inc}$.

The simple expression on the right hand side is due to the identity

$$\big\langle\!\big\langle (\mathsf{Id} - \mathsf{M}_\Sigma)(\gamma^0 U_{\rm inc}, 0, \ldots, 0), \mathfrak{v}\big\rangle\!\big\rangle = \langle\!\langle \mathfrak{u}_{\rm inc}, \mathfrak{v}\rangle\!\rangle\ ,$$

which is a consequence of (3.4) and the fact that $U_{\rm inc}$ solves an interior Helmholtz problem on Ω_*, see (1.1).

The next Lemma paves the way for a regularized form of (3.16).

Lemma 3.1 $\quad \forall \kappa > 0 : \quad \mathbb{M}_\Sigma[\kappa](\mathfrak{u})(\boldsymbol{x}) = 0 \quad \forall \boldsymbol{x} \in \mathbb{R}^d, \quad \forall \mathfrak{u} \in \boldsymbol{\mathcal{ST}}(\Sigma)\ .$

A proof of this result can be found after [6, Lemma 5.1].

Hence, for $\mathfrak{u} \in \boldsymbol{\mathcal{ST}}(\Sigma)$ we can "add zero" in the form of $\mathsf{M}_\Sigma[\kappa_0](\mathfrak{u}) := \gamma^\Sigma \mathbb{M}_\Sigma[\kappa_0](\mathfrak{u}) = 0$ to Formulation 3.1 and convert it into a *regularized formulation.*

Formulation 3.2 *Search* $\mathfrak{u} \in \boldsymbol{\mathcal{ST}}(\Sigma)$:

$$\langle\!\langle (\mathsf{Id} - (\mathsf{M}_\Sigma - \mathsf{M}_\Sigma[\kappa_0]))\,\mathfrak{u}, \mathfrak{v}\rangle\!\rangle = \langle\!\langle \mathfrak{u}_{\rm inc}, \mathfrak{v}\rangle\!\rangle\ , \quad \forall \mathfrak{v} \in \boldsymbol{\mathcal{MT}}(\Sigma). \tag{3.17}$$

Why this formulation deserves the label "regularized" will be elucidated in the next section and in Theorem 4.3.

3.4 New Second-Kind Boundary Integral Formulation in L^2

The advantage of Formulation 3.2 is that it remains well defined on a L^2-based function space.

Definition 3.5 The *skeleton multi-trace L^2-space* is given by

$$\boldsymbol{\mathcal{ML}}^2(\Sigma) := \bigtimes_{i=0}^{N} L^2(\partial\Omega_i) \times L^2(\partial\Omega_i)\,. \tag{3.18}$$

In L^2 the transmission conditions can be expressed as pointwise constraints on functions in the multi-trace space, which motivates the following definition

Definition 3.6 The *single-trace L^2-space* is defined by

$$\begin{aligned}\boldsymbol{\mathcal{SL}}^2(\Sigma) := \big\{&(u_0,\nu_0,\dots,u_N,\nu_N) \in \boldsymbol{\mathcal{ML}}^2(\Sigma) : \\ &u_i\big|_{\Gamma_{ij}} = u_j\big|_{\Gamma_{ij}},\ \nu_i\big|_{\Gamma_{ij}} = -\nu_j\big|_{\Gamma_{ij}},\ \forall j<i\big\}\,.\end{aligned}$$

Of course, sufficiently regular functions in $\boldsymbol{\mathcal{ST}}(\Sigma)$ also belong to $\boldsymbol{\mathcal{SL}}^2(\Sigma)$.

The next theorem provides the polar identity (3.12) in the L^2-setting:

Theorem 3.2

$$\boldsymbol{\mathcal{SL}}^2(\Sigma) = \{\mathfrak{u} \in \boldsymbol{\mathcal{ML}}^2(\Sigma) : \langle\!\langle \mathfrak{u},\mathfrak{v}\rangle\!\rangle = 0,\ \forall \mathfrak{v} \in \boldsymbol{\mathcal{SL}}^2(\Sigma)\}\,.$$

Proof (i) By continuity of the bilinear L^2-pairing we obtain

$$\mathfrak{u},\mathfrak{v} \in \boldsymbol{\mathcal{SL}}^2(\Sigma) \Rightarrow \langle\!\langle \mathfrak{u},\mathfrak{v}\rangle\!\rangle = 0\,,$$

because it holds on the dense subset $\boldsymbol{\mathcal{ST}}(\Sigma)\cap\boldsymbol{\mathcal{ML}}^2(\Sigma) \subset \boldsymbol{\mathcal{SL}}^2(\Sigma)$.

(ii) Fix $\mathfrak{u} = (u_0,\nu_0,\dots,u_N,\nu_N) \in \boldsymbol{\mathcal{ML}}^2(\Sigma)$ and take an arbitrary $\mathfrak{v} = (v_0,\psi_0,\dots,v_N,\psi_N) \in \boldsymbol{\mathcal{SL}}^2(\Sigma)$. We have to show that $\langle\!\langle \mathfrak{u},\mathfrak{v}\rangle\!\rangle = 0$ implies $\mathfrak{u} \in \boldsymbol{\mathcal{SL}}^2(\Sigma)$:

$$0 = \langle\!\langle \mathfrak{u},\mathfrak{v}\rangle\!\rangle \overset{\mathfrak{v}\in\boldsymbol{\mathcal{SL}}^2(\Sigma)}{=} \sum_{j<i}\int_{\Gamma_{ij}} (u_i-u_j)\overline{\psi_i} + (\nu_i+\nu_j)\overline{v_i}\,\mathrm{d}S\,. \tag{3.19}$$

Since this identity holds for all $\mathfrak{v} \in \boldsymbol{\mathcal{SL}}^2(\Sigma)$ it implies $u_i = u_j$ a.e. on Γ_{ij} and $\nu_i = -\nu_j$ a.e. on Γ_{ij} for all $j<i \in \{0,1,\dots,N\}$, respectively. This is equivalent to $\mathfrak{u} \in \boldsymbol{\mathcal{SL}}^2(\Sigma)$. □

A consequence is that Lemma 3.1 carries over to the L^2-setting.

Corollary 3.2 *$\boldsymbol{\mathcal{SL}}^2(\Sigma)$ is a closed subspace of $\boldsymbol{\mathcal{ML}}^2(\Sigma)$.*

A closer scrutiny reveals that taking the difference of boundary integral operators in (3.17) involves a *cancellation of the leading singularities* of their kernels, refer to the proof of Theorem 4.3 for details. This enhances the smoothing properties of the boundary integral operators and yields the following compactness result, whose proof boils down to adapting the ideas of [20, Remark 3.1.3].

Theorem 3.3 *The operator $\mathbf{M}_\Sigma - \mathbf{M}_\Sigma[\kappa_0] : \boldsymbol{\mathcal{ML}}^2(\Sigma) \to \boldsymbol{\mathcal{ML}}^2(\Sigma)$ is compact.*

The bilinear pairing $\langle\!\langle \cdot, \cdot \rangle\!\rangle$ from (3.9) clearly extends to a continuous bilinear form on $\boldsymbol{\mathcal{ML}}^2(\Sigma) \times \boldsymbol{\mathcal{ML}}^2(\Sigma)$. Thus, as a consequence of Theorem 3.3, the bilinear form on the left-hand side of (3.17) is also continuous on $\boldsymbol{\mathcal{ML}}^2(\Sigma) \times \boldsymbol{\mathcal{ML}}^2(\Sigma)$. By density of $\boldsymbol{\mathcal{ML}}^2(\Sigma) \cap \boldsymbol{\mathcal{MT}}(\Sigma) \subset \boldsymbol{\mathcal{ML}}^2(\Sigma)$ we obtain that equation (3.17) holds for all test functions $\mathfrak{v} \in \boldsymbol{\mathcal{ML}}^2(\Sigma)$. Combined with the fact that Lemma 3.1 carries over to the L^2-setting this leads to the "lifted" equivalent of Formulation 3.2:

Formulation 3.3 *Search* $\mathfrak{u} \in \boldsymbol{\mathcal{SL}}^2(\Sigma)$:

$$\langle\!\langle (\mathsf{Id} - (\mathbf{M}_\Sigma - \mathbf{M}_\Sigma[\kappa_0]))\, \mathfrak{u}, \mathfrak{v} \rangle\!\rangle = \langle\!\langle \mathfrak{u}_{\mathrm{inc}}, \mathfrak{v} \rangle\!\rangle \,, \quad \forall \mathfrak{v} \in \boldsymbol{\mathcal{ML}}^2(\Sigma). \tag{3.20}$$

A remedy for the obvious mismatch of trial and test space in Formulation 3.3 is suggested by the following fundamental observation [6, Proposition 5.1].

Theorem 3.4

$$\langle\!\langle (\mathbf{M}_\Sigma - \mathbf{M}_\Sigma[\kappa_0])\, \mathfrak{u}, \mathfrak{v} \rangle\!\rangle = \langle\!\langle \mathfrak{u}, \mathfrak{v} \rangle\!\rangle \,, \quad \forall \mathfrak{u} \in \boldsymbol{\mathcal{ML}}^2(\Sigma),\ \forall \mathfrak{v} \in \boldsymbol{\mathcal{SL}}^2(\Sigma)\,. \tag{3.21}$$

The idea of its proof is to remember the jump relations for the potentials, see [20, Sect. 3.3.1], [16, Thm. 6.11], and to understand that the multi-potential $\mathbb{M}_\Sigma$ features vanishing jumps of Dirichlet and Neumann traces across the interfaces. By density arguments, it does not matter whether we make these considerations in $\boldsymbol{\mathcal{MT}}(\Sigma)$ or in $\boldsymbol{\mathcal{ML}}^2(\Sigma)$. Then appeal to Theorem 3.2 to conclude the assertion. A formal proof can be done exactly like that of [6, Proposition 5.1].

Since $\langle\!\langle \mathfrak{u}_{\mathrm{inc}}, \mathfrak{v} \rangle\!\rangle = 0$ for $\mathfrak{v} \in \boldsymbol{\mathcal{SL}}^2(\Sigma)$, Theorem 3.4 implies that equation (3.3) is trivial for all test functions $\mathfrak{v} \in \boldsymbol{\mathcal{SL}}^2(\Sigma)$. Since $\boldsymbol{\mathcal{SL}}^2(\Sigma)$ is a closed subspace of $\boldsymbol{\mathcal{ML}}^2(\Sigma)$ by Corollary 3.2, it is sufficient to test with elements in *any* complement space $\boldsymbol{\mathcal{SL}}^{2,c}(\Sigma)$ of $\boldsymbol{\mathcal{SL}}^2(\Sigma) \subset \boldsymbol{\mathcal{ML}}^2(\Sigma)$, i.e.,

$$\boldsymbol{\mathcal{ML}}^2(\Sigma) = \boldsymbol{\mathcal{SL}}^2(\Sigma) \oplus \boldsymbol{\mathcal{SL}}^{2,c}(\Sigma)\,.$$

For the sake of easy implementation we choose $\boldsymbol{\mathcal{SL}}^{2,c}(\Sigma) := \boldsymbol{\mathcal{SL}}^{2,\perp}(\Sigma)$, the L^2-orthogonal complement space.

Definition 3.7 (Complement of single-trace L^2 space)

$$\boldsymbol{\mathcal{SL}}^{2,\perp}(\Sigma) := \Big\{ (u_0, \nu_0, \ldots, u_N, \nu_N) \in \boldsymbol{\mathcal{ML}}^2(\Sigma) : \\ u_i\big|_{\Gamma_{ij}} = -u_j\big|_{\Gamma_{ij}},\ \nu_i\big|_{\Gamma_{ij}} = \nu_j\big|_{\Gamma_{ij}},\ j < i \Big\}\,.$$

This gives us another variational formulation equivalent to Formulation 3.3:

Formulation 3.4 *Search* $\mathbf{u} \in \boldsymbol{\mathcal{SL}}^2(\Sigma)$:

$$\langle\!\langle (\mathsf{Id} - (\mathbf{M}_\Sigma - \mathbf{M}_\Sigma[\kappa_0]))\,\mathbf{u}, \mathbf{v} \rangle\!\rangle = \langle\!\langle \mathbf{u}_{\mathrm{inc}}, \mathbf{v} \rangle\!\rangle \;, \quad \forall \mathbf{v} \in \boldsymbol{\mathcal{SL}}^{2,\perp}(\Sigma) \;. \tag{3.22}$$

The straightforward Definition 3.7 reveals the benefit of an L^2-based variational formulation; in [6] an approach set in the original trace spaces was pursued, for which it turned out to be difficult to handle the complement spaces.

Theorem 3.3 implies that the operator $\mathsf{Id} - (\mathbf{M}_\Sigma - \mathbf{M}_\Sigma[\kappa_0])$ is Fredholm with index zero. Therefore, the Formulations (3.3) and (3.4) are variational boundary integral equations of the second kind. Thanks to the Fredholm Alternative (cf. [20, Theorem 4.2.9]) it is sufficient to prove injectivity of the operator on $\boldsymbol{\mathcal{SL}}^2(\Sigma)$ to show existence and uniqueness of solutions.

Unfortunately, a proof for uniqueness has remained elusive so far. The standard approach that works for the case of a uniform scatterer ($N = 1$) and for classical first-kind approaches (see [7, Lemma 3.4]) does not carry over to multi-potentials. However, the numerical experiments of Section 5.1 did not yield the slightest hint at a breakdown at particular wave numbers.

Therefore, henceforth we will make the following assumption:

Assumption 3.1 *We assume that Formulation 3.4 admits a unique solution* $\mathbf{u} \in \boldsymbol{\mathcal{SL}}^2(\Sigma)$.

The subsequent Lemma 3.2 gives us the key result, which is needed to show equivalence of Formulation 3.4 to the original problem (1.2). It is implied by elliptic lifting results [16, Theorem 4.16] and the obvious fact that $\Delta U \in L^2_{\mathrm{loc}}(\mathbb{R}^d)$.

Lemma 3.2 *The solution* U *of* (1.2) *satisfies* $U \in H^2_{\mathrm{loc}}(\mathbb{R}^d)$.

Theorem 3.5 (Equivalence) *Under Assumption 3.1, the solution* $\mathbf{u}$ *of Formulation 3.4 provides the multi-trace* $\gamma^\Sigma U$ *of the solution* U *of the transmission problem* (1.2).

Proof For strongly elliptic partial differential equations with incident plane wave, we know that Dirichlet resp. Neumann data of the solution U, $\mathbf{u} = \gamma^\Sigma U$, lie in $\boldsymbol{\mathcal{SL}}^2(\Sigma)$ (combine the result from Lemma 3.2 with [9, Lemma 3.6]). By construction, the boundary data $\gamma^\Sigma U$ of the unique solution U of (1.2) satisfy equation (3.22). Together with the uniqueness Assumption 3.1 this implies the assertion. □

Obviously, the interface based L^2-skeleton space $\boldsymbol{\mathcal{L}}^2(\Sigma) := \bigtimes_{j<i} L^2(\Gamma_{ij}) \times L^2(\Gamma_{ij})$ is isometrically isomorphic to $\boldsymbol{\mathcal{SL}}^2(\Sigma)$ by the following one-to-one correspondance: any element $\mathbf{u} = (u_{ij}, \nu_{ij})_{j<i} \in \boldsymbol{\mathcal{L}}^2(\Sigma)$ is associated to the

element $\underline{\mathfrak{u}} = (u_0, \nu_0, \ldots, u_N, \nu_N) \in \boldsymbol{\mathcal{SL}}^2(\Sigma)$ with

$$(u_i, \nu_i) = \begin{cases} (u_{ij}, +\nu_{ij}) & \text{on } \Gamma_{ij} \text{ if } i > j \\ (u_{ji}, -\nu_{ji}) & \text{on } \Gamma_{ji} \text{ if } i < j \end{cases}, \; i = 0, \ldots, N\,.$$

Thus, using (3.10), Formulation 3.4 can be rewritten in such a way that ansatz and test functions belong to $\boldsymbol{\mathcal{L}}^2(\Sigma)$.

Formulation 3.5 *Search* $\mathfrak{u} \in \boldsymbol{\mathcal{L}}^2(\Sigma)$:

$$\langle\!\langle (\mathsf{Id} - (\mathsf{M}_\Sigma - \mathsf{M}_\Sigma[\kappa_0]))\, \underline{\mathfrak{u}}, \underline{\mathfrak{v}} \rangle\!\rangle = \langle\!\langle \mathfrak{u}_{\mathrm{inc}}, \underline{\mathfrak{v}} \rangle\!\rangle, \; \forall \mathfrak{v} \in \boldsymbol{\mathcal{L}}^2(\Sigma).$$

4 Boundary Element Discretization

4.1 Boundary Element Spaces

For the Galerkin discretization of the variational problem of Formulation 3.5 we rely on finite dimensional subspaces $\boldsymbol{\mathcal{L}}^2_h(\Sigma) \subset \boldsymbol{\mathcal{L}}^2(\Sigma)$. In contrast to formulations set in $\boldsymbol{\mathcal{ST}}(\Sigma)$, their choice faces no continuity constraints; we merely have to make sure that $\boldsymbol{\mathcal{L}}^2(\Sigma)$-stable sets of basis functions are available.

We opt for conventional boundary element trial and test spaces $\boldsymbol{\mathcal{L}}^2_h(\Sigma)$ that are piecewise polynomial with respect to a finite partition (mesh) $\mathcal{T} = \{\tau_1, \ldots, \tau_{|\mathcal{T}|}\}$ of Σ [20, Sect. 4.1.2]. We assume that $\mathcal{T}$ resolves edges and corners of Σ, and the interfaces Γ_{ij}, in the sense that the closure of every Γ_{ij} agrees with the union of some closed cells of $\mathcal{T}$.

The natural choice for $\boldsymbol{\mathcal{L}}^2_h(\Sigma)$ is $\boldsymbol{\mathcal{L}}^2_{\mathcal{T}}(\Sigma) := \mathcal{S}^{p,-1}_{\mathcal{T}}(\Sigma) \times \mathcal{S}^{p,-1}_{\mathcal{T}}(\Sigma)$, where $\mathcal{S}^{p,-1}_{\mathcal{T}}(\Sigma)$ denotes the set of all discontinuous piecewise polynomial functions of maximal total degree p on the mesh $\mathcal{T}$, see [20, Section 4.1.3] ($d = 3$), [22, Chapter 10] ($d = 2$). For the sake of simplicity, in the sequel we restrict ourselves to $p = 0$, the space of all piecewise constant functions on the mesh $\mathcal{T}$:

$$\mathcal{S}^{0,-1}_{\mathcal{T}}(\Sigma) := \left\{ \psi \in L^\infty(\Sigma) \,\middle|\, \forall \tau \in \mathcal{T} : \psi|_\tau \text{ is constant} \right\},$$

which is a vector space of dimension $|\mathcal{T}| = \#\{\tau \,|\, \tau \in \mathcal{T}\}$.

Remark 4.1 (Approximation of skeleton) *Our theoretical investigations assume exact representation of Σ. Yet, practical computations will invariably substitute the skeleton Σ by a piecewise polynomial interpolant Σ_{disc} [20, Sect. 8.1.1]. Analysis shows that this approximation of Σ does not affect the asymptotic behavior of the discretization error, if one chooses it of high enough order [20, Section 8 (Table 8.3)]. For piecewise constant trial and test functions an approximation of Σ by line segments ($d = 2$) or flat triangles ($d = 3$) is already sufficient. Then normal vectors on individual cells are constant.* △

We also fix an ordering of the cells of the mesh: $\mathcal{T} = \{\tau_1, \tau_2, ..., \tau_{|\mathcal{T}|}\}$, and endow each element with an orientation in such a way, that $\tau_k \in \Gamma_{ij}$ inherits the intrinsic orientation of Γ_{ij}. This choice of orientation is made to keep notation simple, but is essentially arbitrary.

Since $\mathcal{T}_{|\Gamma_{ij}}$ supplies a mesh of Γ_{ij}, the approximation space $\boldsymbol{\mathcal{L}}^2_{\mathcal{T}}(\Sigma)$ can be split into interface contributions

$$\boldsymbol{\mathcal{L}}^2_{\mathcal{T}}(\Sigma) = \bigtimes_{j<i} \mathcal{S}^{0,-1}_{\mathcal{T}}(\Gamma_{ij}) \times \mathcal{S}^{0,-1}_{\mathcal{T}}(\Gamma_{ij}) \subset \boldsymbol{\mathcal{L}}^2(\Sigma) \,, \tag{4.1}$$

where $\mathcal{S}^{0,-1}_{\mathcal{T}}(\Gamma_{ij})$ is the space of $\mathcal{T}_{|\Gamma_{ij}}$-piecewise constant functions on Γ_{ij}.

4.2 Convergence and Conditioning

We consider a sequence $\{\mathcal{T}_\ell\}_{\ell\in\mathbb{N}}$ of skeleton meshes with $h_\ell := \max\{\mathrm{diam}(\tau),\, \tau \in \mathcal{T}_\ell\} \to 0$ as $\ell \to \infty$. It is to satisfy the standard assumptions of quasi-uniformity and shape regularity, see [22, Section 10.1] ($d = 2$) or [20, Section 4.1.2] ($d = 3$) for details. Under these circumstances approximation error estimates for piecewise constants are well known, see [22, Theorem 10.4] ($d = 2$) or [20, Corollary 4.1.34] ($d = 3$):

Theorem 4.1 *Writing $\mathcal{T}_{ij,\ell} := \mathcal{T}_{\ell\,|\Gamma_{ij}}$, $0 \le i < j \le N$, we have for $\sigma \in [-1, 0]$, $s \in [\sigma, 1]$,*

$$\inf_{v\in\mathcal{S}^{0,-1}_{\mathcal{T}_{ij,\ell}}} \|u - v\|_{H^\sigma(\Gamma_{ij})} \le C h_\ell^{\min\{s,1\}-\sigma} |u|_{H^s(\Sigma)} \quad \forall u \in H^s(\Gamma_{ij}) \,,$$

with $C > 0$ depending only on σ, s, and the shape regularity of $\{\mathcal{T}_\ell\}_{\ell\in\mathbb{N}}$.

We denote by $\boldsymbol{\mathcal{L}}^2_\ell(\Sigma)$ the space $\boldsymbol{\mathcal{L}}^2_{\mathcal{T}_l}(\Sigma)$ of piecewise constant functions on $\mathcal{T}_\ell$. Thanks to Theorem 3.3, the abstract theory of Galerkin approximation of coercive linear variational problems [20, Sect. 4.2.3] immediately gives us asymptotic quasi-optimality of the Galerkin solutions of Formulation 3.5 in $\boldsymbol{\mathcal{L}}^2(\Sigma)$.

Theorem 4.2 *Provided that Assumption 3.1 holds, there is $\ell_0 \in \mathbb{N}$ and a constant $C > 0$ independent of ℓ such that a unique Galerkin solution $\mathfrak{u}_\ell \in \boldsymbol{\mathcal{L}}^2_\ell(\Sigma)$ of Formulation 3.5 exists for all $\ell \ge \ell_0$ and satisfies*

$$\|\mathfrak{u} - \mathfrak{u}_\ell\|_{L^2(\Sigma)} \le C \inf_{\mathfrak{v}_\ell\in\boldsymbol{\mathcal{L}}^2_\ell(\Sigma)} \|\mathfrak{u} - \mathfrak{v}_\ell\|_{L^2(\Sigma)} \,. \tag{4.2}$$

Combined with Theorem 4.1, this allows to predict rates of algebraic convergence depending on the smoothness of the Cauchy traces. The best possible rate will be 1.

For $\mathcal{S}^{0,-1}_{\mathcal{T}_\ell}(\Sigma)$ we choose the "canonical" basis $\{|\tau|^{-\frac{1}{2}}\chi_\tau : \tau \in \mathcal{T}_\ell\}$ of locally supported scaled characteristic functions. This basis enjoys the perfect L^2-stability property

$$u_\ell = \sum_\tau \xi_\tau \, |\tau|^{-\frac{1}{2}} \chi_\tau \quad \Rightarrow \quad \sum_\tau |\xi_\tau|^2 = \|u_\ell\|^2_{L^2(\Sigma)} \ . \tag{4.3}$$

Thus, by the continuity of $\mathbf{M}_\Sigma - \mathbf{M}_\Sigma[\kappa_0] : \boldsymbol{\mathcal{ML}}^2(\Sigma) \to \boldsymbol{\mathcal{ML}}^2(\Sigma)$ and the asymptotic stability of Formulation 3.5 from Theorem 4.2 we can conclude that for ℓ big enough the Euclidean condition numbers $\mathrm{cond}_2(\mathbf{G}_\ell)$ of the Galerkin matrices $\mathbf{G}_\ell \in \mathbb{C}^{2|\mathcal{T}_\ell|,2|\mathcal{T}_\ell|}$ for Formulation 3.5 on $\boldsymbol{\mathcal{L}}^2_\ell(\Sigma)$ (equipped with the basis of scaled characteristic functions introduced above) are bounded independently of ℓ, if Assumption 3.1 holds true.

4.3 Computation of Galerkin matrices

Write $\mathcal{T}_{ij} := \mathcal{T}_{|\Gamma_{ij}}$ for the set of cells having support on Γ_{ij}. Number the cells of $\mathcal{T}_{ij}$, which induces a numbering of the basis functions of $\boldsymbol{\mathcal{L}}^2_{\mathcal{T}}(\Sigma)$ supported on Γ_{ij}. We dub this the *local* numbering. To connect it to the global numbering of basis functions of $\boldsymbol{\mathcal{L}}^2_{\mathcal{T}}(\Sigma)$, we rely on the index mapping matrices $\boldsymbol{L}_{\Gamma_{\mathrm{ij}}} \in \mathbb{R}^{|\mathcal{T}_{ij}|\times|\mathcal{T}|}$ defined through

$$(\boldsymbol{L}_{\Gamma_{\mathrm{ij}}})_{lk} := \begin{cases} 1 & \text{, if } \tau_k \subset \Gamma_{ij} \quad \text{and} \quad l \text{ is the local index of } \tau_k \in \mathcal{T}_{ij} \ , \\ 0 & \text{else.} \end{cases} \tag{4.4}$$

Now we are in a position to express the $\boldsymbol{\mathcal{L}}^2_{\mathcal{T}}(\Sigma)$-Galerkin matrix $\boldsymbol{G} \in \mathbb{C}^{2|\mathcal{T}|,2|\mathcal{T}|}$ of Formulation 3.5:

$$\boldsymbol{G} = \sum_{j<i} \left(\begin{pmatrix} \boldsymbol{L}_{\Gamma_{\mathrm{ij}}} & \mathbf{0} \\ \mathbf{0} & \boldsymbol{L}_{\Gamma_{\mathrm{ij}}} \end{pmatrix}^T \begin{pmatrix} \mathbf{0} & \boldsymbol{M}_{ij} \\ \boldsymbol{M}_{ij} & \mathbf{0} \end{pmatrix} \right.$$
$$\left. - \sum_{q<p} \begin{pmatrix} \boldsymbol{L}_{\Gamma_{\mathrm{pq}}} & \mathbf{0} \\ \mathbf{0} & \boldsymbol{L}_{\Gamma_{\mathrm{pq}}} \end{pmatrix}^T \underbrace{\begin{pmatrix} \boldsymbol{W}^{pq}_{ij} & \boldsymbol{K}'^{pq}_{ij} \\ -\boldsymbol{K}^{pq}_{ij} & \boldsymbol{V}^{pq}_{ij} \end{pmatrix}}_{\boldsymbol{C}^{pq}_{ij}} \right) \begin{pmatrix} \boldsymbol{L}_{\Gamma_{\mathrm{ij}}} & \mathbf{0} \\ \mathbf{0} & \boldsymbol{L}_{\Gamma_{\mathrm{ij}}} \end{pmatrix} ,$$

where $\boldsymbol{M}_{ij}$ is the diagonal local mass matrix (multiplied by a factor 2) for Γ_{ij}, and the $|\mathcal{T}_{ij}| \times |\mathcal{T}_{pq}|$-blocks of $\boldsymbol{C}^{pq}_{ij} \in \mathbb{C}^{2|\mathcal{T}_{ij}|,2|\mathcal{T}_{pq}|}$ arise from the Galerkin discretization on $\mathcal{S}^{0,-1}_{\mathcal{T}_{ij}}(\Gamma_{ij}) \times \mathcal{S}^{0,-1}_{\mathcal{T}_{ij}}(\Gamma_{pq})$ of sesqui-linear expressions of the form

$$(u, v) \mapsto \int_{\Gamma_{pq}} \int_{\Gamma_{ij}} Z^{pq}_{ij}(\boldsymbol{x}, \boldsymbol{y}) u(\boldsymbol{y}) \overline{v(\boldsymbol{x})} \, \mathrm{d}S(\boldsymbol{y}) \mathrm{d}S(\boldsymbol{x}) \ ,$$

where Z^{pq}_{ij} stands for a kernel that is different for the different matrices $\boldsymbol{W}^{pq}_{ij}$, $\boldsymbol{K}'^{pq}_{ij}$, $\boldsymbol{K}^{pq}_{ij}$, and $\boldsymbol{V}^{pq}_{ij}$. In concrete terms, with the notation indicating the relationship with the matrices, and $\boldsymbol{r} := \boldsymbol{x} - \boldsymbol{y}$, in the different cases the kernel

Z_{ij}^{pq} reads

$$Z_{ij}^{pq} \quad \leftrightarrow \quad \begin{aligned} \mathsf{v}_{ij}^{pq}(\boldsymbol{x},\boldsymbol{y}) &:= 2\left(\Phi_{\kappa_i}(\boldsymbol{r}) - \Phi_{\kappa_j}(\boldsymbol{r})\right) , \\ \mathsf{k}_{ij}^{pq}(\boldsymbol{x},\boldsymbol{y}) &:= 2\left(\mathbf{n}_i(\boldsymbol{y})\cdot\mathbf{grad}_{\boldsymbol{y}}(\Phi_{\kappa_i}(\boldsymbol{r}) - \Phi_{\kappa_j}(\boldsymbol{r}))\right) , \\ \mathsf{k}'^{pq}_{ij}(\boldsymbol{x},\boldsymbol{y}) &:= 2\left(\mathbf{n}_p(\boldsymbol{x})\cdot\mathbf{grad}_{\boldsymbol{x}}(\Phi_{\kappa_i}(\boldsymbol{r}) - \Phi_{\kappa_j}(\boldsymbol{r}))\right) , \\ \mathsf{w}_{ij}^{pq}(\boldsymbol{x},\boldsymbol{y}) &:= -2\left(\mathbf{n}_p(\boldsymbol{x})\cdot\mathbf{grad}_{\boldsymbol{x}}\left(\mathbf{n}_i(\boldsymbol{y})\cdot\mathbf{grad}_{\boldsymbol{y}}(\Phi_{\kappa_i}(\boldsymbol{r}) - \Phi_{\kappa_j}(\boldsymbol{r}))\right)\right) . \end{aligned} \tag{4.5}$$

Thus, the contributions to $\boldsymbol{C}_{ij}^{pq}$ of the basis functions associated with cells $\tau_k \in \Gamma_{pq}$, $\tau_l \in \Gamma_{ij}$ are of the following form

$$\begin{aligned} &\int_{\tau_k}\int_{\tau_l} \mathsf{w}_{ij}^{pq}(\boldsymbol{x},\boldsymbol{y})\mathrm{d}S(\boldsymbol{y})\mathrm{d}S(\boldsymbol{x}) , \quad \int_{\tau_k}\int_{\tau_l} \mathsf{k}'^{pq}_{ij}(\boldsymbol{x},\boldsymbol{y})\mathrm{d}S(\boldsymbol{y})\mathrm{d}S(\boldsymbol{x}) , \\ -&\int_{\tau_k}\int_{\tau_l} \mathsf{k}_{ij}^{pq}(\boldsymbol{x},\boldsymbol{y})\mathrm{d}S(\boldsymbol{y})\mathrm{d}S(\boldsymbol{x}) , \quad \int_{\tau_k}\int_{\tau_l} \mathsf{v}_{ij}^{pq}(\boldsymbol{x},\boldsymbol{y})\mathrm{d}S(\boldsymbol{y})\mathrm{d}S(\boldsymbol{x}) . \end{aligned} \tag{4.6}$$

To understand the origin of the kernels in (4.5), and, in particular, why κ_0 does no longer enter, we elaborate the formulas for a particular entry of $\boldsymbol{G}$ corresponding to trial and test functions $\tau_l \in \Gamma_{rs}, r > s$ and $\tau_k \in \Gamma_{pq}, p > q$ in the "Dirichlet component" of $\mathfrak{u}$ and $\mathfrak{v}$ of Formulation 3.5.

Take two elements $\mathfrak{u} = (u_{ij},\nu_{ij})_{j<i}, \mathfrak{v} = (v_{ij},\psi_{ij})_{j<i} \in \boldsymbol{\mathcal{L}}^2(\Sigma)$, with $(u_{ij},\nu_{ij}) = 0$ if $(i,j) \neq (r,s)$, $(v_{ij},\psi_{ij}) = 0$ if $(i,j) \neq (p,q)$, and $(u_{rs},\nu_{rs}) = (\chi_{\tau_l},0)$, $(v_{pq},\psi_{pq}) = (\chi_{\tau_k},0)$. Considering the associated multi-traces $\underline{\mathfrak{u}} = (\mathfrak{u}_0,\dots,\mathfrak{u}_N)$ and $\underline{\mathfrak{v}} = (\mathfrak{v}_0,\dots\mathfrak{v}_N)$ we have on the one hand $\mathfrak{u}_i = 0$ if $i \neq r,s$ and $\mathfrak{u}_r = \mathfrak{u}_s = (\chi_{\tau_l},0)$, and on the other hand $\mathfrak{v}_j = 0$ if $j \neq p,q$ and $\mathfrak{v}_p = -\mathfrak{v}_q = (\chi_{\tau_k},0)$. Plugging these observations in Formulation 3.5 yields

$$\begin{aligned} &\langle\!\langle \left(\mathsf{Id} - \mathbf{M}_\Sigma + \mathbf{M}_\Sigma[\kappa_0]\right)\underline{\mathfrak{u}},\underline{\mathfrak{v}} \rangle\!\rangle \\ &= 0 - \sum_{j=p,q}\sum_{i=r,s} \left\langle\!\!\left\langle \gamma^j\left(\mathbb{G}_i[\kappa_i] - \mathbb{G}_i[\kappa_0]\right)\mathfrak{u}_i,\mathfrak{v}_j\right\rangle\!\!\right\rangle_{\mathcal{H}(\partial\Omega_j)} \\ &= 0 - 2\sum_{i=r,s} \left\langle \gamma_N^p\left(\mathbb{G}_i[\kappa_i] - \mathbb{G}_i[\kappa_0]\right)\mathfrak{u}_i,\chi_{\tau_k}\right\rangle_{\Gamma_{pq}} \\ &= 0 - 2\left\langle \gamma_N^p\left(\mathbb{G}_r[\kappa_r] - \mathbb{G}_r[\kappa_0] + \mathbb{G}_s[\kappa_s] - \mathbb{G}_s[\kappa_0]\right)\mathfrak{u}_r,\chi_{\tau_k}\right\rangle_{\Gamma_{pq}} \\ &\overset{-\mathbf{n}_r=\mathbf{n}_s}{=} - \left\langle -2\,\gamma_N^p\left(\mathbb{D}_r[\kappa_r] - \mathbb{D}_r[\kappa_s]\right)\chi_{\tau_l},\,\chi_{\tau_k}\right\rangle_{\Gamma_{pq}} \\ &= -\int_{\tau_k}\int_{\tau_l} \mathsf{w}_{rs}^{pq}(\boldsymbol{x},\boldsymbol{y})\mathrm{d}S(\boldsymbol{y})\mathrm{d}S(\boldsymbol{x}) , \end{aligned}$$

where the definition of w_{ij}^{pq} can be found in (4.5).

The next theorem confirms that the kernels from (4.5) are regular enough to ensure that the integrals in (4.6) are well defined, at least as improper integrals.

Theorem 4.3 (Regularity of kernels) *The kernels* $\mathsf{v}_{ij}^{pq}(\boldsymbol{x},\boldsymbol{y})$, $\mathsf{k}_{ij}^{pq}(\boldsymbol{x},\boldsymbol{y})$ *and* $\mathsf{k}'^{pq}_{ij}(\boldsymbol{x},\boldsymbol{y})$ *defined in* (4.5) *are continuous. The kernel* $\mathsf{w}_{ij}^{pq}(\boldsymbol{x},\boldsymbol{y})$ *is weakly singular for* $\boldsymbol{x}=\boldsymbol{y}$.

Proof We simply establish series expansions of the regularized kernels involved in the integral operator $\mathbf{M}_\Sigma - \mathbf{M}_\Sigma[\kappa_0]$ (see (4.5)). We give the complete proof for the case $d=2$, while in the case $d=3$ we examine only v_{ij}^{pq} and leave the remainder to the reader, since the reasoning is analogous to the case $d=2$.

Case $d=2$**:** We use properties of the Bessel and Hankel functions J_α, Y_α and $H_\alpha^{(1)}$, respectively, $\alpha\in\mathbb{N}$, see, for example, [3] and [1]. First of all we study the kernel $\mathsf{v}_{ij}^{pq}(\boldsymbol{x},\boldsymbol{y})$. To simplify notation, we denote by $r:=|\boldsymbol{x}-\boldsymbol{y}|$ the distance between the poins $\boldsymbol{x}$ and $\boldsymbol{y}$ and obtain

$$\begin{aligned}
&\frac{\mathsf{i}}{4}\big(H_0^{(1)}(\kappa_i r)-H_0^{(1)}(\kappa_j r)\big)\\
&\quad=\frac{\mathsf{i}}{4}\left(J_0(\kappa_i r)-J_0(\kappa_j r)+\mathsf{i}Y_0(\kappa_i r)-\mathsf{i}Y_0(\kappa_j r)\right)\\
&\quad=-\frac{1}{2\pi}\left[\sum_{s=1}^{\infty}\frac{(-4)^{-s}}{s!^2}r^{2s}\left\{\left(\log(r)-\sum_{\nu=1}^{s}\frac{1}{\nu}-\left(\psi(1)+\frac{\pi}{2}\mathsf{i}\right)\right)\left(\kappa_i^{2s}-\kappa_j^{2s}\right)\right.\right.\\
&\qquad\left.\left.+\log\left(\frac{1}{2}\kappa_i\right)\kappa_j^{2s}-\log\left(\frac{1}{2}\kappa_j\right)\kappa_j^{2s}\right\}+\log\frac{\kappa_i}{\kappa_j}\right].
\end{aligned}\tag{4.7}$$

Thus, the "most singular term" is $r^2\log(r)$ and the kernel v_{ij}^{pq} is obviously continuous. Manipulating the kernel $k_{ij}^{pq}(\boldsymbol{x},\boldsymbol{y})$ one obtains:

$$\begin{aligned}
&\frac{\mathsf{i}}{4}\left(-H_1^{(1)}(\kappa_i r)\kappa_i+H_1^{(1)}(\kappa_j r)\kappa_j\right)\frac{-\mathbf{n}_i(\boldsymbol{y})\cdot\boldsymbol{r}}{r}\\
&=\sum_{s=0}^{\infty}\frac{(-4)^{-s}}{s!(s+1)!}r^{2s+1}\left[\left\{\mathsf{i}-\frac{2}{\pi}\log(r)+\frac{\psi(s+1)+\psi(s+2)}{\pi}\right\}\left(\kappa_i^{2s+2}-\kappa_j^{2s+2}\right)\right.\\
&\qquad\left.+\frac{2}{\pi}\log\left(\frac{1}{2}\kappa_j\right)\kappa_j^{2s+2}-\frac{2}{\pi}\log\left(\frac{1}{2}\kappa_i\right)\kappa_i^{2s+2}\right]\frac{-\mathbf{n}_i(\boldsymbol{y})\cdot\boldsymbol{r}}{8r}
\end{aligned}\tag{4.8}$$

Therefore also in this case we end up with a continuous kernel with "most singular term" $r\log(r)$.

The expansion of the kernel $\mathsf{k}'^{pq}_{ij}(\boldsymbol{x},\boldsymbol{y})$ is obtained analogously to the one of $\mathsf{k}_{ij}^{pq}(\boldsymbol{x},\boldsymbol{y})$ above. We only need to replace $\mathbf{n}_i(\boldsymbol{y})$ by $-\mathbf{n}_p(\boldsymbol{x})$ in the result 4.8 to end up with the expansion of $\mathsf{k}'^{pq}_{ij}(\boldsymbol{x},\boldsymbol{y})$.

Finally, we analyze the kernel $\mathsf{w}_{ij}^{pq}(\boldsymbol{x},\boldsymbol{y})$. It can be rewritten as

$$\begin{aligned}
&\frac{\mathsf{i}}{4}\mathbf{n}_p(\boldsymbol{x})\cdot\mathbf{grad}_{\boldsymbol{x}}\left[\left(-H_1^{(1)}(\kappa_i r)\kappa_i+H_1^{(1)}(\kappa_j r)\kappa_j\right)\frac{\mathbf{n}_i(\boldsymbol{y})\cdot\boldsymbol{r}}{r}\right]\\
&=\frac{\mathsf{i}}{4}\left(\kappa_i^2H_0^{(1)}(\kappa_i r)-\frac{\kappa_i}{r}H_1^{(1)}(\kappa_i r)\right.\\
&\qquad\left.-\kappa_j^2H_0^{(1)}(\kappa_j r)+\frac{\kappa_j}{r}H_1^{(1)}(\kappa_j r)\right)\frac{\mathbf{n}_p(\boldsymbol{x})\cdot\boldsymbol{r}\;\mathbf{n}_i(\boldsymbol{y})\cdot\boldsymbol{r}}{r^2}
\end{aligned}$$

$$+\frac{\mathsf{i}}{4}\left(\kappa_i H_1^{(1)}(\kappa_i r)-\kappa_j H_1^{(1)}(\kappa_j r)\right)\left(\frac{\mathbf{n}_p(\boldsymbol{x})\cdot\mathbf{n}_i(\boldsymbol{y})}{r}-\frac{\mathbf{n}_p(\boldsymbol{x})\cdot\boldsymbol{r}\;\mathbf{n}_i(\boldsymbol{y})\cdot\boldsymbol{r}}{r^2}\right)$$

just by writing out the derivatives in full. This leads to the final form

$$\begin{aligned}
&\left\{\sum_{s=1}^{\infty}\frac{(-4)^{-s}}{(s!)^2}r^{2s}Q_s(\log(r),\kappa_i,\kappa_j)\right.\\
&\qquad\left.+\left(\mathsf{i}+\frac{2\psi(1)}{\pi}\right)\left(\kappa_i^2-\kappa_j^2\right)\right\}\frac{\mathbf{n}_p(\boldsymbol{x})\cdot\boldsymbol{r}\,\mathbf{n}_i(\boldsymbol{y})\cdot\boldsymbol{r}}{4r^2}\\
&+\left\{\sum_{s=1}^{\infty}\frac{(-4)^{-s}}{(s!)^2}r^{2s}\tilde{Q}_s(\log(r),\kappa_i,\kappa_j)+\left(\frac{1}{\pi}(\psi(s+1)+\psi(s+2))\right)\left(\kappa_i^2-\kappa_j^2\right)\right.\\
&\qquad\left.+\mathsf{i}\right\}\left(\frac{\mathbf{n}_p(\boldsymbol{x})\cdot\mathbf{n}_i(\boldsymbol{y})}{8}-\frac{\mathbf{n}_p(\boldsymbol{x})\cdot\boldsymbol{r}\,\mathbf{n}_i(\boldsymbol{y})\cdot\boldsymbol{r}}{4r^2}\right)-\frac{2}{\pi}\left\{\log(r)\left(\kappa_i^2-\kappa_j^2\right)\right.\\
&\qquad\left.+\log\left(\frac{1}{2}\kappa_i\right)\kappa_i^2-\log\left(\frac{1}{2}\kappa_j\right)\kappa_j^2\right\}\frac{\mathbf{n}_p(\boldsymbol{x})\cdot\mathbf{n}_i(\boldsymbol{y})}{8},
\end{aligned}\tag{4.9}$$

$$\begin{aligned}
Q_s(\log(r),\kappa_i,\kappa_j)&=-\frac{2}{\pi}\left(\log(r)-\frac{\pi}{2}\mathsf{i}-\psi(1)-\left(\sum_{\nu=1}^{s}\frac{1}{\nu}\right)\right)\left(\kappa_i^{2s+2}-\kappa_j^{2s+2}\right)\\
&\quad-\frac{2}{\pi}\log\left(\frac{1}{2}\kappa_i\right)\kappa_i^{2s+2}+\frac{2}{\pi}\log\left(\frac{1}{2}\kappa_j\right)\kappa_j^{2s+2},\\
\tilde{Q}_s(\log(r),\kappa_i,\kappa_j)&=\left(-\frac{2}{\pi}\log(r)+\mathsf{i}+\frac{1}{\pi}(\psi(s+1)+\psi(s+2))\right)\left(\kappa_i^{2s+2}-\kappa_j^{2s+2}\right)\\
&\quad-\frac{2}{\pi}\log\left(\frac{1}{2}\kappa_i\right)\kappa_i^{2s+2}+\frac{2}{\pi}\log\left(\frac{1}{2}\kappa_j\right)\kappa_j^{2s+2}.
\end{aligned}$$

Since $Q_s(\log(r),\kappa_i,\kappa_j)$ and $\tilde{Q}_s(\log(r),\kappa_i,\kappa_j)$ are linear in $\log(r)$, the expression (4.9) is continuous except for the weakly singular term involving $\log(r)$ in the second to last line.

Case $d=3$**:** The kernel v_{ij}^{pq} has the simple form

$$\frac{1}{4\pi r}\left(\exp(\mathsf{i}\kappa_i r)-\exp(\mathsf{i}\kappa_j r)\right)=\frac{1}{4\pi}\sum_{k=1}^{\infty}\frac{(\mathsf{i}\kappa_i)^{k+1}-(\mathsf{i}\kappa_j)^{k+1}}{(k+1)!}r^k+\mathsf{i}(\kappa_i-\kappa_j),$$

from which continuity as a function of $r=|\boldsymbol{x}-\boldsymbol{y}|$ is obvious. □

Since the kernels involve differences of terms of about the same size for $r\approx 0$, cancellation becomes a key issue in an implementation (see also Fig. 4.1). We overcome this problem by using truncated versions of the series expansions derived in the proof of Theorem 4.3. If $r:=|\boldsymbol{x}-\boldsymbol{y}|$ is sufficiently large, we simply evaluate the difference of the kernels according to (4.5). If r is close to 0, i.e. the condition

$$r|\kappa_i-\kappa_j|<\mathrm{tol},\quad 0<\mathrm{tol}<1\quad\text{a small constant},\tag{4.10}$$

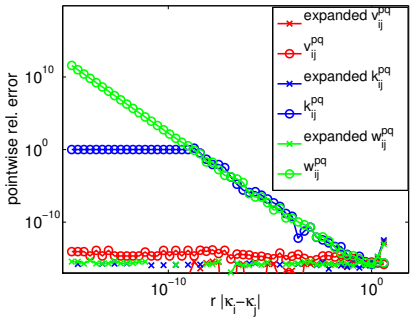

(a) $\kappa_i = 3$, $\kappa_j = 5$, $\alpha(\mathbf{n}_i(\boldsymbol{y}), \boldsymbol{r}) = 45°$, $\alpha(\mathbf{n}_j(\boldsymbol{x}), \boldsymbol{r}) = 120°$, $N_{\text{trunc}} = 30$

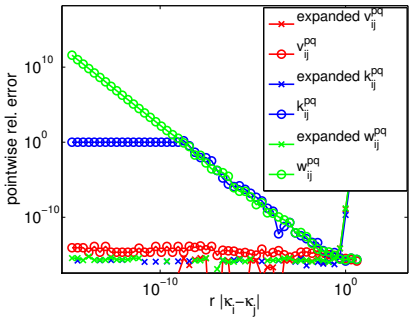

(b) $\kappa_i = 3$, $\kappa_j = 5$, $\alpha(\mathbf{n}_i(\boldsymbol{y}), \boldsymbol{r}) = 45°$, $\alpha(\mathbf{n}_j(\boldsymbol{x}), \boldsymbol{r}) = 120°$, $N_{\text{trunc}} = 8$

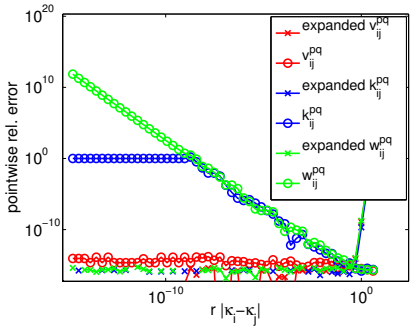

(c) $\kappa_i = 3$, $\kappa_j = 5$, $\alpha(\boldsymbol{n}_i(\boldsymbol{y}), \boldsymbol{r}) = 95°$, $\alpha(\mathbf{n}_j(\boldsymbol{x}), \boldsymbol{r}) = 85°$, $N_{\text{trunc}} = 8$

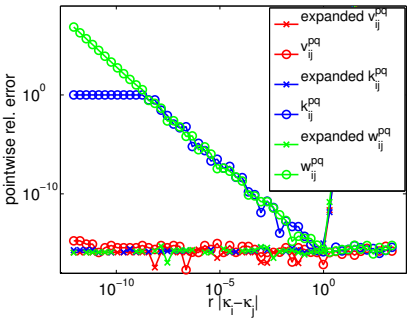

(d) $\kappa_i = 3$, $\kappa_j = 1000$, $\alpha(\mathbf{n}_i(\boldsymbol{y}), \boldsymbol{r}) = 45°$, $\alpha(\mathbf{n}_j(\boldsymbol{x}), \boldsymbol{r}) = 120°$, $N_{\text{trunc}} = 8$

Fig. 4.1: **Convergence of series expansions:** depicted are the relative pointwise errors as a function of $r|\kappa_i - \kappa_j|$, where $r := |\boldsymbol{x} - \boldsymbol{y}|$, of the expansions found in the proof of Theorem 4.3, truncated at N_{trunc}. The reference solutions are calculated with MATHEMATICA with very high precision. $\alpha(\mathbf{n}_i(\boldsymbol{y}), \boldsymbol{r})$ denotes the angle between $\mathbf{n}_i(\boldsymbol{y})$ and $\boldsymbol{r} := \boldsymbol{x} - \boldsymbol{y}$.

is satisfied, we resort to the truncated series expansions. If condition (4.10) is met for some fixed tolerance we may truncate the series after a fixed number of terms and still have a small guaranteed relative truncation error. Experiments documented in Figure 4.1 showed, that an appropriate number of terms for the truncated series for $d = 2$ is $N_{\text{trunc}} = 8$, together with $\text{tol} = 0.4$ in (4.10).

The previous discussion gives us a numerically stable evaluation of the weakly singular kernels in (4.6). A suitable quadrature rule to integrate these nonsmooth kernels when the cells $\tau_k, \tau_l \in \mathcal{T}$ are neighbors is given by geometric composite Gauss-Legendre quadrature proposed in [21]. The integrals over the truncated series expansion for elements that coincide can easily be evaluated analytically.

5 Numerical Results in Two Dimensions

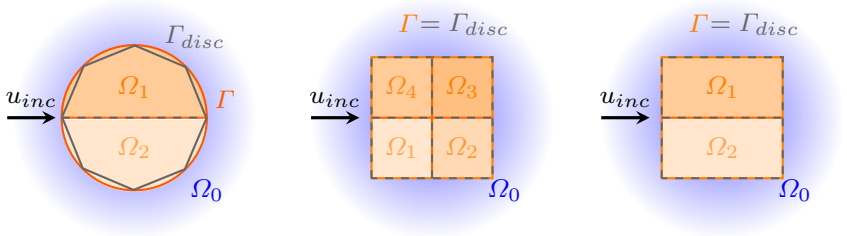

(a) two half discs of radius $r = 0.4$

(b) four quarts of a square of side length $s = 0.5$

(c) two halfs of a square of side length $s = 0.5$

Fig. 5.1: Geometries for numerical experiments

We implemented the Galerkin discretization of Formulation 3.5 based on piecewise constant trial and test functions, which has been presented in Section 4. Unless stated otherwise, we use equidistant meshes on the interfaces. We consider the three different geometries sketched in Figure 5.1. In all computations, the incident field is given by the plane wave $\mathbf{u}_{\text{inc}} := \exp(\mathrm{i}\kappa_0 \boldsymbol{d}\cdot\boldsymbol{x})$, $\boldsymbol{d} = (1,\,0)^T$, $\boldsymbol{x} \in \mathbb{R}^2$.

5.1 Stability

The numerical experiments in this section have been conducted for two half disks of Fig. 5.1 (a), and are meant to analyze the stability of the discretized versions of our new second-kind Formulation 3.4 to justify Assumption 3.1.

In a first experiment we try to detect potential breakdowns of the new formulation, which should manifest itself as spikes in the Euclidean condition numbers of the Galerkin matrices $\boldsymbol{G}$ for certain wave numbers. In Figure 5.2 we observe localized regions with large condition numbers, see Fig. 5.2. To obtain more detailed information about the origin of the spike depicted in Fig. 5.2(b), we fix the wave numbers $(\kappa_0, \kappa_1, \kappa_2) = (9.538, 1, 0.72)$ (depicted by the cyan $\mathbf{x}$ in Fig. 5.2) located in the region where we observe the largest condition numbers and solve the radiation eigenvalue problem

$$-\Delta\mathbf{u} - (\beta\kappa(\boldsymbol{x}))^2\mathbf{u} = 0 \quad \text{in } \mathbb{R}^2\,, \quad \beta \in \mathbb{C}\,. \tag{5.1}$$

Of particular interest is the region around $\beta = 1$ represented by the intersection of the blue ($\mathsf{Imag}(\beta) = 0$) and red line ($\mathsf{Real}(\beta) = 1$) in Fig. 5.3. In this case we are exactly in the setting where the Galerkin matrices display a peak in the condition number (see Fig. 5.2(b)). Since we observe a numerical eigenvalue of (5.1) very close very close to the real axis and $\beta = 1$, the peak depicted in Fig. 5.2 seems be triggered by an *open resonance*. Conversely, no such eigenvalues close to the real axis are observed for combinations of wave numbers that do

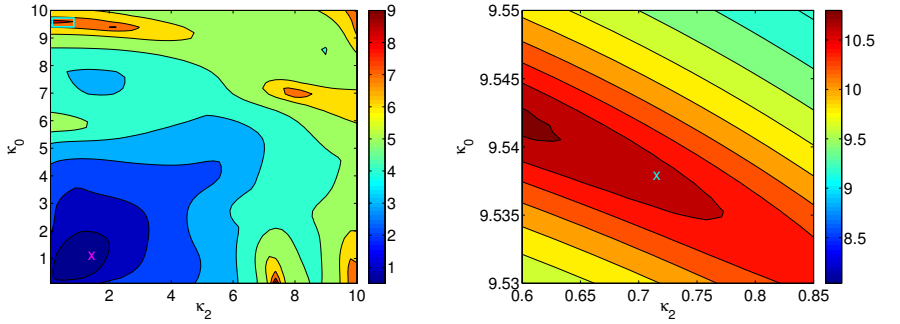

(a) global situation

(b) zoom into area marked by cyan rectangle in the upper left of subfigure (a)

Fig. 5.2: (Logarithms of)**Euclidean condition numbers of Galerkin matrix for various wave numbers:** The Galerkin matrix of the second-kind formulation for the situation of two half discs (Fig. 5.1 (a)) with equidistant mesh, $|\mathcal{T}| = 480$, is used. The wave number $\kappa_1 = 1$ is fixed, while $\kappa_0, \kappa_2 \in (0.1 : \frac{99}{500} : 10)$ (for (a)) resp. $\kappa_0 \in (9.53 : \frac{1}{100} : 9.55)$, $\kappa_2 \in (0.6 : \frac{35}{200} : 0.85)$ (for (b)).

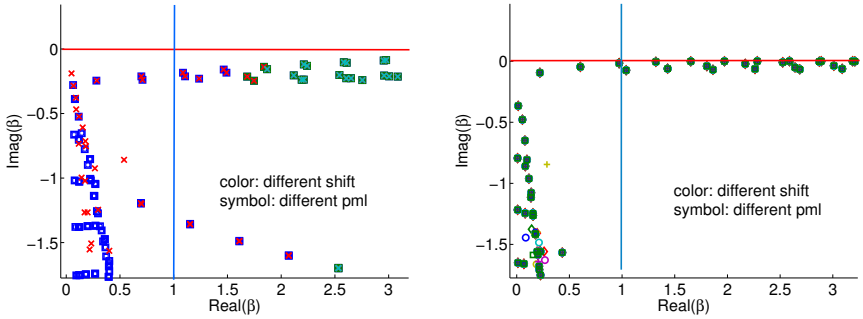

(a) non-resonant situation

(b) near resonance situation

Fig. 5.3: **Numerically computed open resonances** found by an Arnoldi algorithm implemented in the *hp* finite element code NGSolve [2]. The different symbols stand for complex eigenvalues of (5.1), see [14] for more detailed explanations.

not give rise to ill-conditioned discrete problems, see Fig. 5.3(a), where we used $(\kappa_0, \kappa_1, \kappa_2) = (0.7, 1, 1.22)$ (depicted by the pink **x** in Fig. 5.2) for a numerical study. This is strong evidence that whenever the discrete second-kind formulation shows signs of instability, this merely reflects inherent instability of the scattering problem. This gave us faith in Assumption 3.1.

5.2 Convergence

In this section we compare the convergence of the $L^2(\Sigma)$-norm of the error of the approximate Dirichlet and Neumann data obtained from our new second-kind formulation with the results calculated with the classical STF approach, see [7, Section 3.2] or [23]. The latter were obtained by a conforming Galerkin discretization using $\mathcal{S}^{1,0}_{\mathcal{T}}(\Sigma) \times \mathcal{S}^{0,-1}_{\mathcal{T}}(\Sigma) \subset \boldsymbol{\mathcal{L}}^2(\mathcal{T})$ for ansatz and test space. To get a reliable reference solution, we computed highly accurate solutions of the scattering problems by the hp-FEM code Concepts [24]. In Figure 5.4 we plot $L^2(\Sigma)$-errors for the geometries sketched in Fig. 5.1 versus number of mesh cells. The errors computed with different reference solutions agree well.

The estimated algebraic rates of convergence of the computed errors match the rates predicted by the a priori estimates of Section 4.2. Comparing the results for the Neumann data, the rates computed with the new second-kind approach are by $\frac{1}{2}$ larger than the rates observed for the discrete first-kind STF. However, the errors of the Dirichlet data of the first-kind approach converge with rates that larger by 1. The reason is, that we use continuous piecewise linear boundary elements to approximate the Dirichlet traces for the classical method, while our new formulation relies on piecewise constants only.

We observe competitive accuracy also for Dirichlet data when applying a cheap postprocessing procedure to the Dirichlet solution from our new second-kind approach, see Fig. 5.4. Details are presented in Section 5.3.

5.3 Postprocessing of Dirichlet Data

Though we rely on discontinuous approximation, the exact Dirichlet traces are known to be continuous. We tried to recover a continuous approximation and applied an $L^2(\Sigma)$-orthogonal projection onto the boundary element space $\mathcal{S}^{1,0}_{\mathcal{T}}(\Sigma)$ of continuous piecewise linear functions to the Dirichlet part of the piecewise constant Galerkin solution $\mathbf{u}_h \in \mathcal{S}^{0,-1}_{\mathcal{T}}(\Sigma) \times \mathcal{S}^{0,-1}_{\mathcal{T}}(\Sigma)$.

Throughout, this postprocessing yielded substantially improved approximations of the Dirichlet data that show enhanced rates of convergence and match the accuracy of solutions of the classical Galerkin STF, see Figures 5.4 and Section 5.2.

A theoretical explanation for this effect is still missing. Further investigations by numerical experiments hint that the order of convergence of the projected approximate Dirichlet traces deteriorates on general meshes. The result provides some evidence that the improved convergence rate due to postprocessing is a superconvergence phenomenon on regular meshes.

5.4 Conditioning of Galerkin Matrices

In a second numerical experiment, we investigate the dependence of the condition numbers on the mesh width. In Section 4.2 we concluded that the condition number of the Galerkin matrix corresponding to our new second-kind

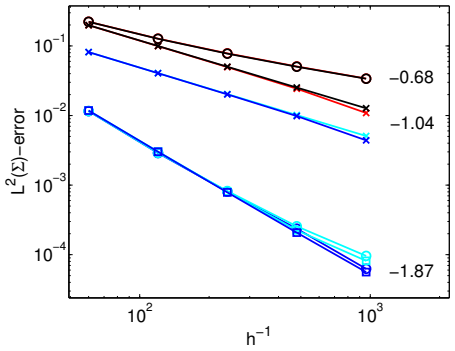

(a) two half discs, $\kappa_0 = 3$, $\kappa_1 = 1$, $\kappa_2 = 5$

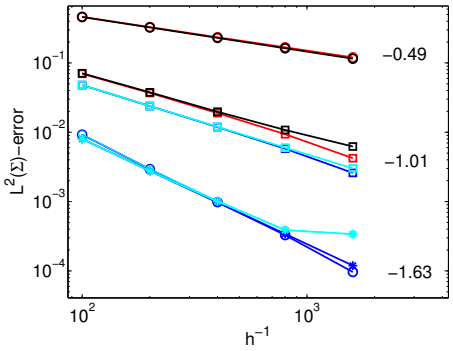

(b) four quarts of a square, $\kappa_0 = 1$, $\kappa_1 = 10$, $\kappa_2 = 2$

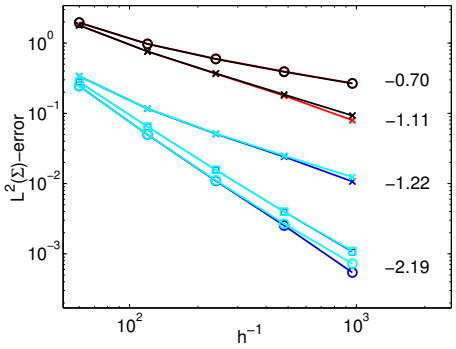

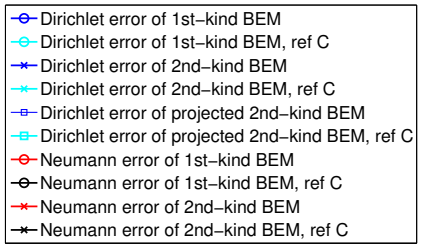

(c) two halfs of a square, $\kappa_0 = 3$, $\kappa_1 = 1, \kappa_2 = 5$, $\kappa_3 = 2$, $\kappa_4 = 3$

Fig. 5.4: **Convergence in $L^2(\Sigma)$-norm** on equidistant meshes with $\frac{3}{2}5 \cdot 2^i$ cells (scatterer composed of two materials) resp. $\frac{5}{2}5 \cdot 2^i$, $i = 3, 4, ..., 8$ elements (four materials). The error norms obtained from the classical STF approach are marked with circles ($\circ$), while the graphs calculated with the second-kind approach are marked with squares ($\square$) and asterisk (*) (postprocessed data). The graphs colored in dark blue represent the data which use the solution of highest resolution as a reference, while the cyan graphs correspond to the errors with respect to the data calculated with CONCEPTS. The errors of the Neumann data are plotted in red (reference solution is the one of highest resolution) and black (wrt. CONCEPTS-solution). The graphs are annotated by estimated rates of convergence.

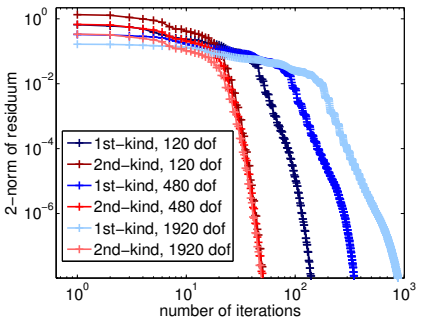

(a) two half discs, $\kappa_0 = 3$, $\kappa_1 = 1$, $\kappa_2 = 5$

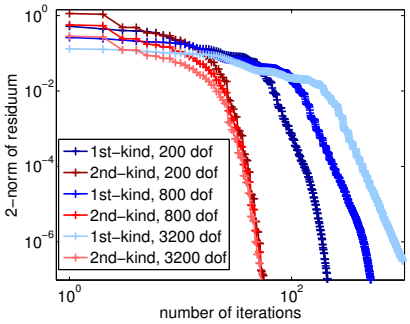

(b) four quarts of a square, $\kappa_0 = 1$, $\kappa_1 = 10$, $\kappa_2 = 2$

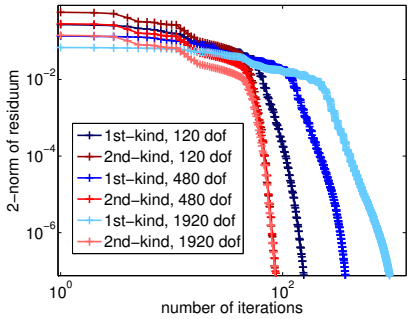

(c) two halfs of a square, $\kappa_0 = 3$, $\kappa_1 = 1$, $\kappa_2 = 5$, $\kappa_3 = 2$, $\kappa_4 = 3$

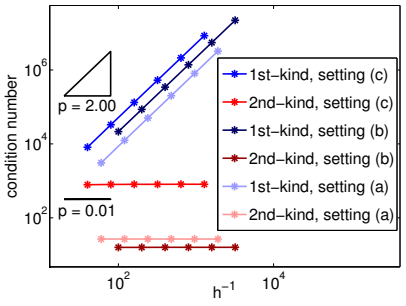

(d) condition numbers of all geometries

Fig. 5.5: **Euclidean condition numbers of Galerkin matrices with respect to $h_{\mathcal{T}}^{-1}$ and performance of GMRES on Galerkin matrices** for different numbers of degrees of freedom (dof, highlighted by different colours). Initial guess used for GMRES is $\boldsymbol{x}_0 = \mathbf{0}$. The expression "setting (a)" (resp. (b) or (c)) in subfigure (d) refers to the geometric setting given in the particular subfigure (a) (resp. (b) or (c)).

formulation is independent of the mesh width $h_{\mathcal{T}}$ of our discretization. This is observed in Fig. 5.5 (d), while for the first-kind approach the condition number increases quadratically when refining the mesh (cf. [20, Section 4.5 & Cor. 6.4.14]). It leads to significantly reduced numbers of iteration of iterative solvers like GMRES for the second-kind approach (see Fig. 5.5 (a), (b) and (c)).

Acknowledgment

The authors would like to thank K. Schmidt for assistance with CONCEPTS [24], and A. Schädle for providing the implementation of the eigenproblem solver in NGSOLVE [2].

References

1. *Digital Library of Mathematical Functions*. http://dlmf.nist.gov/, accessed 2011-08-29.
2. *NGSolve Finite Element Library*. http://sourceforge.net/apps/mediawiki/ngsolve, accessed 2012-05-02.
3. M. Abramowitz and I.A. Stegun. *Handbook of mathematical functions with formulas, graphs, and mathematical tables*, volume 55. Dover publications, 1964.
4. John M. Ball, Yves Capdeboscq, and Basang Tsering Xiao. On uniqueness for time harmonic anisotropic Maxwell's equations with piecewise regular coefficients. *Math. Moodels Meth. Appl. Sci.*, 2012. arXiv:1201.2006v1 [math.AP].
5. A. Barnett and L. Greengard. A new integral representation for quasi-periodic scattering problems in two dimensions. *BIT Numerical Mathematics*, 51(1):67–90, 2011.
6. X. Claeys. A single trace integral formulation of the second kind for acoustic scattering. Research Report 2011-14, Seminar for Applied Mathematics, ETH Zürich, 2001.
7. X. Claeys, R. Hiptmair, and C. Jerez-Hanckes. Multi-trace boundary integral equations. Report 2012-20, SAM, ETH Zürich, Zürich, Switzerland, 2012. Contribution to "Direct and Inverse Problems in Wave Propagation and Applications", I. Graham, U. Langer, M. Sini, M. Melenk, eds., De Gruyter.
8. D. Colton and R. Kress. *Inverse Acoustic and Electromagnetic Scattering Theory*, volume 93 of *Applied Mathematical Sciences*. Springer, Heidelberg, 2nd edition, 1998.
9. M. Costabel. Boundary integral operators on Lipschitz domains: Elementary results. *SIAM Journal on Mathematical Analysis*, 19:613, 1988.
10. M. Costabel and M. Dauge. Maxwell and Lamé eigenvalues on polyhedra. *Math. Methods Appl. Sci.*, 22(3):243–258, 1999.
11. L. Greengard and J.Y. Lee. Short note: Stable and accurate integral equation methods for scattering problems with multiple material interfaces in two dimensions. *Journal of Computational Physics*, 231(6):2389–2395, 2012.
12. R.F. Harrington. Boundary integral formulations for homogeneous material bodies. *J. Electromagnetic Waves and Applications*, 3(1):1–15, 1989.
13. C. Hazard and M. Lenoir. On the solution of time-harmonic scattering problems for Maxwell's equations. *SIAM J. Math. Anal.*, 27(6):1597–1630, 1996.
14. T. Hohage and L. Nannen. Hardy space infinite elements for scattering and resonance problems. SIAM J. Numer. Anal., 47(2):972–996, 2009.
15. R. Kress and GF Roach. Transmission problems for the Helmholtz equation. *Journal of Mathematical Physics*, 19(6):1433–1437, 1978.
16. W. McLean. *Strongly Elliptic Systems and Boundary Integral Equations*. Cambridge University Press, Cambridge, UK, 2000.
17. C. Müller. *Foundations of the mathematical theory of electromagnetic waves*. Springer Berlin, Heidelberg, New York, 1969.
18. A.J. Poggio and E.K. Miller. Integral equation solution of three-dimensional scattering problems. In R. Mittra, editor, *Computer Techniques for Electromagnetics*, chapter 4, pages 159–263. Pergamon, New York, 1973.
19. V. Rokhlin. Solution of acoustic scattering problems by means of second kind integral equations. *Wave Motion*, 5(3):257–272, 1983.
20. S.A. Sauter and C. Schwab. *Boundary element methods*. Springer, 2011.
21. C. Schwab. Variable order composite quadrature of singular and nearly singular integrals. *Computing*, 53(2):173–194, 1994.
22. O. Steinbach. *Numerical approximation methods for elliptic boundary value problems: finite and boundary elements*. Springer Verlag, 2008.

23. T. Von Petersdorff. Boundary integral equations for mixed Dirichlet, Neumann and transmission problems. *Mathematical methods in the applied sciences*, 11(2):185–213, 1989.
24. Mengyu Wang, Christian Engström, Kersten Schmidt, and Christian Hafner. On high-order FEM applied to canonical scattering problems in plasmonics. *J. Comput. Theor. Nanosci.*, 8:1–9, 2011.

Recent Research Reports

Nr.	Authors/Title

2013-03 X. Claeys and R. Hiptmair
Integral Equations on Multi-Screens

2013-04 V. Kazeev and M. Khammash and M. Nip and Ch. Schwab
Direct Solution of the Chemical Master Equation using Quantized Tensor Trains

2013-05 R. Kaeppeli and S. Mishra
Well-balanced schemes for the Euler equations with gravitation

2013-06 C. Schillings
A Note on Sparse, Adaptive Smolyak Quadratures for Bayesian Inverse Problems

2013-07 A. Paganini and M. López-Fernández
Efficient convolution based impedance boundary condition

2013-08 R. Hiptmair and C. Jerez-Hanckes and J. Lee and Z. Peng
Domain Decomposition for Boundary Integral Equations via Local Multi-Trace Formulations

2013-09 C. Gittelson and R. Andreev and Ch. Schwab
Optimality of Adaptive Galerkin methods for random parabolic partial differential equations

2013-10 M. Hansen and C. Schillings and Ch. Schwab
Sparse Approximation Algorithms for High Dimensional Parametric Initial Value Problems

2013-11 F. Mueller and Ch. Schwab
Finite Elements with mesh refinement for wave equations in polygons

2013-12 R. Kornhuber and Ch. Schwab and M. Wolf
Multi-Level Monte-Carlo Finite Element Methods for stochastic elliptic variational inequalities